Optical design of a dynamic focus catheter for high-resolution endoscopic optical coherence tomography

Panomsak Meemon,* Kye-Sung Lee, Supraja Murali, and Jannick Rolland
CREOL, College of Optics and Photonics, University of Central Florida, Orlando, Florida 32816, USA
*Corresponding author: pmeemon@creol.ucf.edu

Received 19 December 2007; revised 13 March 2008; accepted 31 March 2008;
posted 3 April 2008 (Doc. ID 91016); published 28 April 2008

The optical system design of a dynamic focus endoscopic probe for optical coherence tomography is reported. The dynamic focus capability is based on a liquid lens technology that provides variable focus by changing its curvatures in response to an electric field variation. The effects of a cylindrical exit window present, in practice, for a catheter were accounted for. Degradation in image quality caused by this window was corrected to get diffraction limited imaging performance. As a result, the dynamically focusing catheter with a lateral resolution ranging from 4 to 6 μm through an ~5 mm imaging distance was designed without mechanically refocusing the system. © 2008 Optical Society of America
OCIS codes: 220.4830, 170.2150, 170.3890, 170.4500.

1. Introduction

Optical coherence tomography (OCT) is a noninvasive high-resolution and high sensitivity depth-resolved imaging technique [1]. It is promising for a variety of diagnostic and surgical applications. Axial resolution is determined by the coherence length that depends on the spectrum width of the light source, while the transverse resolution depends on the numerical aperture of the objective lens. Endoscopic optical coherence tomography (EOCT) combines endoscopy with OCT to offer axial depth perception with high sensitivity as well as high spatial resolution for endoscopic imaging. EOCT is suitable for imaging within tubular organs such as the vascular system, the gastrointestinal tract, the breast duct, and the urinary tract [2].

Importantly, the highest lateral resolution is given at the focus of the optics and remains invariant only within the confocal parameter that decreases inversely and quadratically with the numerical aperture (NA) of the optics. Therefore, in applications where a range of focus positions is required, lateral resolution is currently sacrificed to ensure the range of imaging. As a consequence, high-resolution depth imaging is currently limited by the lack of invariant transverse resolution in OCT throughout the depth of imaging. As in all technologies, the clinical applications set the critical parameters for imaging, which can significantly differ across applications. For example, state of the art endoscopy OCT currently implemented clinically for cardiovascular imaging utilizes an 0.8 mm diameter catheter with 8–10 μm axial resolution and 30 μm lateral resolution [3]. For cardiovascular imaging, lateral resolution is not the driving parameter, speed is the critical parameter; thus, while at the expense of resolution, this clinical catheter of less than 1 mm in diameter has been designed to image 1 to 5 mm arteries, a strict requirement for clinical practice. If speed together with high lateral resolution for various artery sizes could be obtained, it would naturally also benefit cardiovascular imaging. For cancer screening or guided biopsy, however, resolution in both axial and lateral dimensions is a critical parameter; thus, there is a keen interest in the development of ultra high-resolution endoscopy OCT, achieving resolution of the order of 1 to 5 μm, which corresponds to current resolutions in histopathology. In this case, while small size catheters

0003-6935/08/132452-06$15.00/0

may be required for imaging lungs, breast, and prostate tissues, to name a few, catheters a few millimeters in diameter can also find direct application, such as for the GI track.

What is believed to be the first side-imaging endoscopic probe for OCT was proposed by Tearney *et al.* [4] with a 1.1 mm diameter. A 38 μm lateral resolution and a 20 μm axial resolution were reported, and an OCT image of *in vitro* human saphenous vein acquired by the authors' probe was presented. The circumferential scanning was achieved by rotating the whole probe using a gear system and rotary optical coupling at the proximal end. Almost at the same time, Tran *et al.* [5] and Herz *et al.* [6] reported the use of micromotors at the distal end of the probe to achieve circumferential scanning without rotating the whole probe. However, the overall probe size can be limited by the size of the micromotor. Tran *et al.* reported a 2.4 mm diameter probe with a resolution of approximately 9.5 μm axially and 13 μm laterally, while Herz *et al.* reported a 5 mm diameter probe with a resolution of 5 μm axially and 8 μm laterally.

Ideally, axial resolution is quasi-invariant throughout the imaging sample as long as the imaging interferometer is balanced for equal dispersion in both arms of the interferometer [7]. On the other hand, to achieve high lateral resolution, one needs to design imaging optics with a high NA while minimizing and balancing residual aberrations. For a high-resolution endoscopic probe, axial chromatic aberration can cause a decrease in the effective bandwidth of the light returning from a particular depth inside the sample. Therefore, achromatization of the probe is required not only to improve the lateral resolution but also to maintain the axial resolution. Tumlinson *et al.* [8,9] reported the use of an optical system design to achieve an achromatized endoscopic probe with a 4.4 μm FWHM lateral spot size at the focus. The probe was designed to operate in a push–pull longitudinally scanning mode with an imaging depth of 0.5 mm.

Nevertheless, the use of a high NA leads to a small depth of focus and the working range of the EOCT (i.e., the high lateral resolution is only maintained close to the focus position). In all these technologies, the lateral resolution reported is at the focus of the imaging probe and degrades inversely and quadratically with the NA of the optics outside the confocal parameter. To maintain a high lateral resolution throughout the depth scanning range, one needs to refocus the imaging optics to fully benefit from the high NA across the full depth of the sample [10]. Doing so with mechanically moving components prohibits high speed scanning and real time imaging [6]. Xie *et al.* [11] proposed the use of a gradient-index (GRIN) lens rod to dynamically adjust the focus of the endoscopic probe. They investigated two different commercially available rod lengths of 127 and 219 mm; however, in either case, the length and the nonflexible nature of the GRIN lens rod may limit the areas of application. Recently, Lee *et al.* [12] investigated the use of Bessel beam imaging using an axicon lens embedded in an optical system design; results show approximately 6 μm invariant lateral resolution and invariant peak intensity throughout a 1.2 mm imaging depth. The probe can be as small as 2 mm, which is currently limited by a circumferential scanning microelectromechanical systems (MEMS) motor at the distal end of the probe. Using external rotors, the probe can be less than 1 mm. This invariant resolution comes at the cost of lower illumination power at each focal position as compared to a conventional focusing lens; yet, a large depth of focus was obtained.

In this study, we investigate the use of a dynamic focusing lens in the optical design of a circumferential scanning probe for EOCT that is capable of remotely controlling the focus position in real time while maintaining a good image quality throughout the depth penetration range.

2. Design Task

The catheter was designed to be used in an OCT system that utilizes a Ti:sapphire (Ti:Sa) laser source with a FWHM spectral width of 120 nm centered at 800 nm, corresponding to an ~2.5 μm axial resolution in air. A circumferential imaging probe was designed using a 2 mm fold mirror attached with a 1.9 mm micromotor at the distal end to rotate the beam 360° [5,6]. To advance the technology an order of magnitude in resolution in comparison to commercial devices, we aimed for a NA of approximately 0.10 that corresponds to less than 10 μm lateral resolution throughout the working depth range, and we designed the optics to reach the diffraction limit. A factor that significantly limits the image quality and resolution is a cylindrical transparent exit window, which causes astigmatism that increases as a function of the window thickness and the distance from the window to the focus position. To remedy this problem, the design utilizes a microlens after the fold mirror to compensate for astigmatism caused by this cylindrical window.

Figure 1 and Table 1 show the optical layout and specifications of the designed dynamic focus catheter. The first element is a liquid lens (ARCTIC 320, Varioptic [13]) that is capable of changing its focal length from 44 mm to 1 m according to an applied voltage (i.e., up to 60 V) within 100 ms. The technology is still being developed to achieve yet higher speeds [14]. The optical power of the liquid lens as a function of an applied voltage was measured and plotted as shown in Fig. 2. The variable focal length overcomes the limitation on depth of focus while using the system at high NA. Also, for small optics of less than 1 mm diameter as needed for endoscopy, the liquid lens may be replaced by a custom design liquid crystal lens that can operate at significantly higher speeds for this small size [10]. For liquid crystal lens technology, the smaller the diameter of the lens, the faster the lens can operate.

A doublet as a combination of SF4 and LAKL12 glass from the Schott catalog, as an example, was

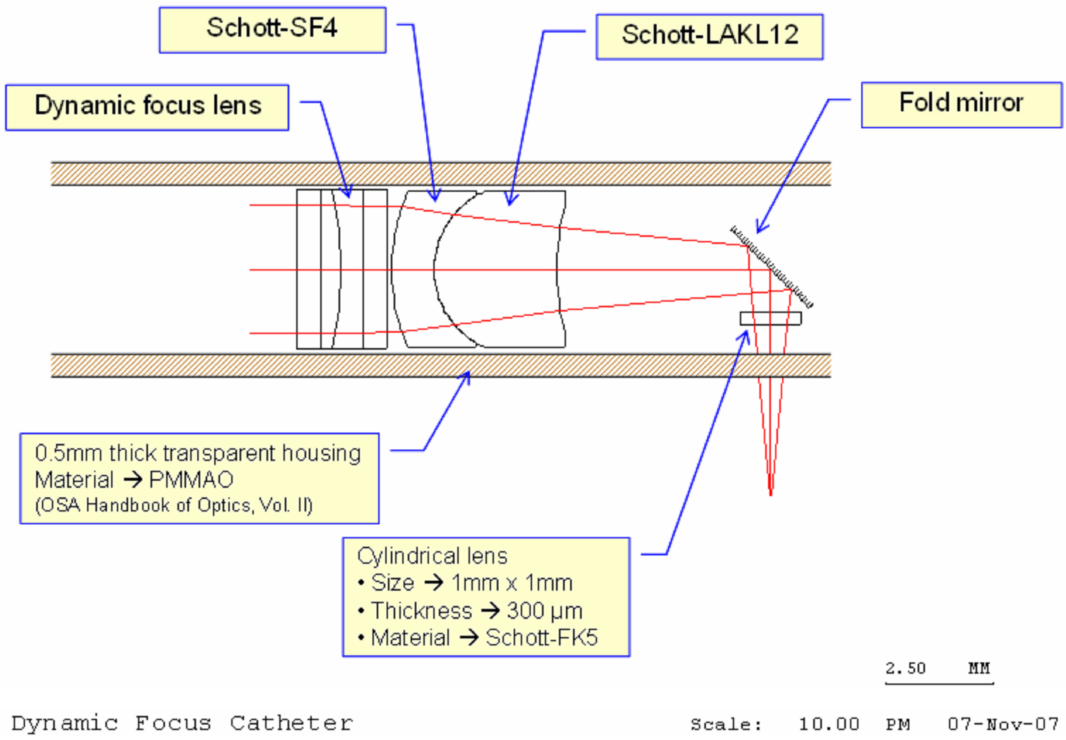

Fig. 1. (Color online) Catheter design layout.

added between the liquid lens and the reflector in order to shorten the catheter length. This configuration leads to a high NA, and the use of a doublet minimizes the axial chromatic aberration throughout the working distance as shown in Fig. 3. The overall ray aberration is shown, however, to be optimum at an ~1.5 mm working distance. In addition, a miniature 1 mm × 1 mm cylindrical lens (Schott FK5) that is 300 μm thick was added after the fold mirror to precompensate the astigmatism caused by the cylindrical window. This lens is attached and rotated together with the fold mirror.

The housing material was chosen to be a polymethylmethacrylate (PMMA), which is transparent in the wavelength range from the ultraviolet (UV) to the near infrared (NIR), easy to fabricate into a product with various shapes, of reasonable cost, and biologically compatible [15,16]. In this design we used a PMMA that is transparent in the ~365–1014 nm wavelength region with an ~1.492 refractive index [17]. The transparent housing allows a fully 360° field of view in lateral scanning. The catheter was designed, optimized, and analyzed using CODE V software (Optical Research Associates, Pasadena, California). The clear aperture diameter of the liquid lens is 3 mm, and the catheter was designed to have an overall diameter equal to 5 mm, as currently limited by the size of the liquid lens. Fig-

Table 1. Design Specification

Fixed parameters					
Source	Ti:Sa laser: 800 nm center wavelength, 120 nm FWHM				
Field of view	On axis with 360° circumferential scan				
Entrance pupil diameter	3 mm				
Physical length	12 mm (excluding collimator and micromotor)				
Overall diameter	5 mm				
Estimated % transmission	>85%[a]				
Dynamic parameters					
Working distance (mm)[b]	0.5	1.5	3.0	4.5	5.5
Numerical aperture	0.12	0.11	0.10	0.09	0.08
Diffraction limited resolution (μm)[c]	4.07	4.44	4.88	5.42	6.10

[a]Based on 94% transmission of the liquid lens, 99% transmission of the doublet and the cylindrical lens, 95% transmission of the mirror, and 98% transmission of the housing window.
[b]Distance from the outer surface to the imaging plane.
[c]Based on the Rayleigh criterion.

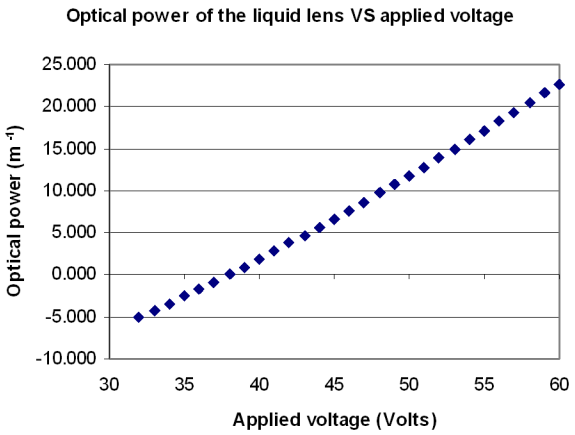

Fig. 2. (Color online) Optical power of the liquid lens as a function of the applied voltage.

ure 4 shows the catheter's layout at three different focus positions.

3. Effects of the Cylindrical Exit Window

Without the cylindrically shaped exit window the lateral resolution, as verified by a two-point source separation analysis, was almost diffraction limited throughout the working range. When accounting for the exit window, the lateral point spread function (PSF) was severely degraded by astigmatism, particularly at the maximum scanning depth of 5 mm, as shown in Fig. 5(a). The aberration caused by the exit window not only degraded the lateral resolution but also reduced the Strehl ratio (SR) leading to a decrease in system sensitivity when the sample was far away from the exit window.

The challenge was how to optimize for this astigmatism throughout the working range while performing the dynamic scan of the imaging plane. Doing so by further minimizing the window thickness was not practically feasible. As shown in Fig. 5(a), the PSF was degraded very fast even with a 50 μm thick window. In this design, we added a cylindrical microlens right after the fold mirror to compensate for the effect of the cylindrical window. The PSF after compensation was dramatically improved as shown in Fig. 5(b) and led to invariant resolution throughout the 5 mm working range. A key component is the attachment of the microlens to the rotating mirror to enable the ~360° scan.

4. Performance

The lateral resolution of the system was assessed at each focal plane throughout the working range starting from 0.5 mm from the last surface of the system, which is the outer surface of the probe, to 5.5 mm from that surface yielding an ~5 mm working range. To estimate the lateral resolution, the FWHM of the PSF at arbitrarily imaging planes was measured as shown in Figs. 6(a)–6(e). Furthermore, using the two-point source separation analysis in CODE V, the system is shown to resolve ~4 μm separation at the close focal plane and 5.5 μm separation at the far focal plane as verified in Figs. 6(f)–6(j). Table 2 summarizes the lateral resolutions, the modulation transfer function, and the SRs through the working range.

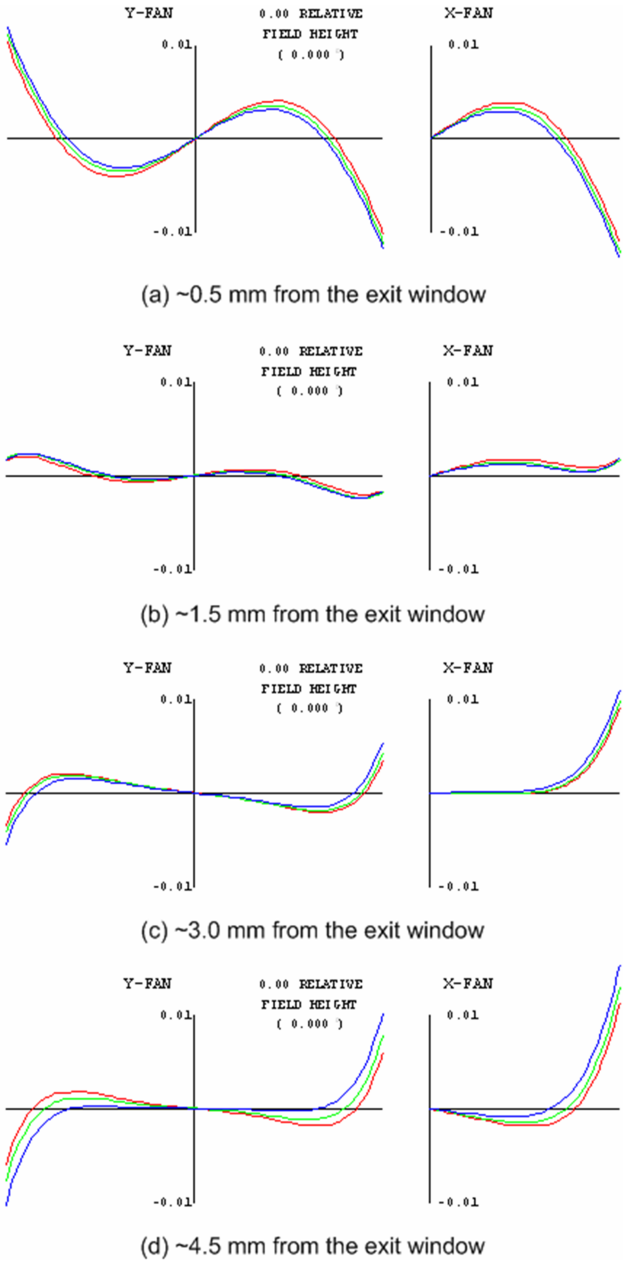

Fig. 3. (Color online) Ray aberration curves at arbitrary focuses plotted within $\pm 10\,\mu$m maximum scale. The chromatic aberration was optimized at the working distances of 0.5, 1.5, and 3 mm; a slight degradation is observed at a distance of ~4.5 mm from the exit window.

5. Fabrication and Assembly Tolerances

In addition, the fabrication and assembly tolerances, together with compensations, were analyzed using the precision quality from Optimax Systems, Ontario, New York, as tolerance limits as shown in Table 3.

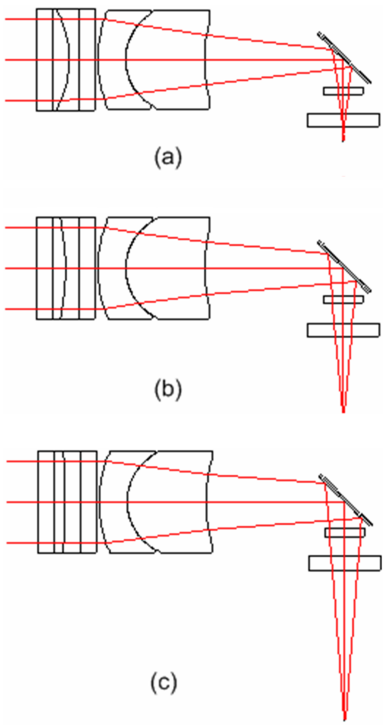

Fig. 4. (Color online) Dynamic focus catheter's layout at three different focus positions; (a) ~0.5 mm, (b) ~3.0 mm, and (c) ~5.5 mm from the outer surface of the exit window.

When operating at proximal focus (i.e., 0.5 mm from the exit window), the probable drop in MTF was less than 11% measured at 100 cycles/mm with the image plane used as a compensator. The necessary displacement of the imaging plane as a compensator was estimated to be around ±0.2 mm. At the distal focus (i.e., 5.5 mm from the exit window), the probable drop in MTF was 12% at 100 cycles/mm with a probable change of the imaging plane of ~±0.3 mm. The drop in MTF was less than 15% and meets the as-built

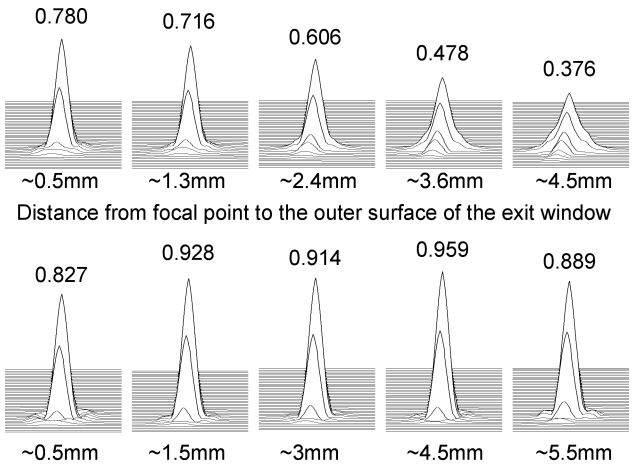

Fig. 5. PSF and SR throughout the working range: top, without the cylindrical microlens and using an already ultrathin 50 μm window thickness; bottom, with a cylindrical microlens and a 500 μm window thickness.

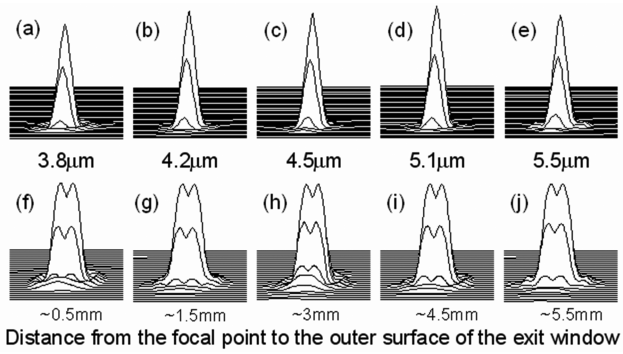

Fig. 6. (a)–(e) PSFs and the corresponding estimated FWHM as indicated by the numbers at the bottom of each PSF. (f)–(j) Resolvability as verified by a two-point source with a separation equal to the corresponding FWHM.

specification in both cases. The slight shift in the image plane can be calibrated once the probe is built. By further tightening the assembly tolerances, this shift could also be further minimized at the expense of increased fabrication cost.

6. Conclusion and Discussion

A high lateral resolution and long working range dynamic focusing probe without mechanical refocusing for an EOCT was designed using a dynamic focusing liquid lens. The doublet was used to minimize the axial chromatic aberration as well as to reduce the overall focal length of the system. Hence, we achieved a probe's length of 12 mm from the first surface of the liquid lens to the fold mirror. The image quality of the system at the far focal plane was severely affected by the transparent cylindrical window that is needed to protect the catheter when acquiring the image inside a tubular sample. This aberration can be compensated for by adding a cylindrical microlens that can correct astigmatism caused by the window regardless of its thickness. With this design, diffraction limited resolution was achieved over a 5 mm imaging distance. The lateral resolution is less than 6 μm with more than an 0.8 Strehl ratio over the 5 mm scanning range (i.e., ~4 μm with an 0.84 Strehl ratio at the proximal focus, and ~6 μm with a 0.9 Strehl ratio at the distal focus).

In clinical imaging situations, the sample size can be varied based on the application. For example, an artery or the GI track can vary in size across locations or across various patients. Combining a dynamic focus probe with a high speed OCT enables imaging at invariant high lateral resolution as the sample size is naturally varying. The ability to dynamically change the focus does not only help maintain a high lateral resolution but also improve the system sensitivity as demonstrated by prior work [6,10].

Future work includes investigating the fabrication of this small probe given that the tolerance analysis yields promising results. Understanding the limits of what can be achieved in downscaling this design to a millimeter or less in overall diameter is also the goal of future work to establish the potential extension of

Table 2. Dynamic Focusing Performance Throughout the Working Range: Lateral Resolution as Determined by the FWHM of the PSF, Averaged MTF at 100 cycles/mm, and SR at Best Focus

Imaging distance[a] (mm)	~0.5	~1.5	~3.0	~4.5	~5.5
Resolution (μm)	3.8	4.1	4.6	5.1	5.5
MTF (%)	~43	~50	~45	~40	~35
SR	0.827	0.928	0.914	0.959	0.889

[a]As measured from the exit window to the focal plane.

Table 3. Fabrication and Assembly Tolerance Analysis

Imaging distance[a] (mm)	0.5	1.5	3.0	4.5	5.5
Probable MTF drop (%)	11	10	12	13	12
Probable shift of focus (mm)	0.21	0.23	0.25	0.29	0.3

[a]As measured from the exit window to the focal plane.

this design to imaging applications beyond the larger tubular structures such as the GI track.

This research is supported by the Florida Photonics Center of Excellence, the University of Central Florida I^{2}Laboratory Fellowship and the Royal Thai Government. We thank Optical Research Associates for the student license that enabled this research in optical system design.

References

1. D. Huang, E. A. Swanson, C. P. Lin, J. S. Schuman, W. G. Stinson, W. Chang, M. R. Hee, T. Flotte, K. Gregory, C. A. Puliafito, and J. G. Fujimoto, "Optical coherence tomography," Science **254**, 1178–1181 (1991).
2. Z. Yaqoob, J. Wu, E. J. McDowell, X. Heng, and C. H. Yang, "Methods and application areas of endoscopic optical coherence tomography," J Biomed. Opt. **11**, 063001 (2006).
3. G. J. Tearney, Department of Pathology, Massachusetts General Hospital, (personal communication, 2007).
4. G. J. Tearney, S. A. Boppart, B. E. Bouma, M. E. Brezinski, N. J. Weissman, J. F. Southern, and J. G. Fujimoto, "Scanning single-mode fiber optic catheter-endoscope for optical coherence tomography," Opt. Lett. **21**, 543–545 (1996).
5. P. H. Tran, D. S. Mukai, M. Brenner, and Z. P. Chen, "*In vivo* endoscopic optical coherence tomography by use of a rotational micro-electromechanical system probe," Opt. Lett. **29**, 1236–1238 (2004).
6. P. R. Herz, Y. Chen, A. D. Aguirre, K. Schneider, P. Hsiung, J. G. Fujimoto, K. Madden, J. Schmitt, J. Goodnow, and C. Petersen, "Micromotor endoscope catheter for *in vivo*, ultrahigh-resolution optical coherence tomography," Opt. Lett. **29**, 2261–2263 (2004).
7. K.-S. Lee, A. C. Akcay, T. Delemos, E. Clarkson, and J. P. Rolland, "Dispersion control with a Fourier-domain optical delay line in a fiber-optic imaging interferometer," Appl. Opt. **44**, 4009–4022 (2005).
8. A. R. Tumlinson, J. K. Barton, J. McNally, A. Unterhuber, B. Hermann, H. Sattman, and W. Drexler, "An achromatized endoscope for ultrahigh-resolution optical coherence tomography," Proc SPIE **5861**, 586110 (2005).
9. A. R. Tumlinson, B. Povazay, L. P. Hariri, J. McNally, A. Unterhuber, B. Hermann, H. Sattmann, W. Drexler, and J. K. Barton, "*In vivo* untrahigh-resolution optical coherence tomography of mouse colon with an achomatized endoscope," J. Biomed. Opt. **11**, 064003-1 (2006).
10. S. Murali, K. S. Lee, and J. P. Rolland, "Invariant resolution dynamic focus OCM based on liquid crystal lens," Opt. Express **15**, 15854–15862 (2007).
11. T. Xie, S. Guo, and Z. P. Chen, "GRIN lens rod based probe for endoscopic spectral domain optical coherence tomography with fast dynamic focus tracking," Opt. Express **14**, 3238–3246 (2006).
12. K. S. Lee, L. Wu, H. Xie, O. Ilegbusi, M. Costa, and J. P. Rolland, "A 5 mm catheter for constant resolution probing in Fourier domain optical coherence endoscopy," Proc. SPIE, **6432**, 64320B (2007).
13. The specification can only be obtained directly from Varioptic (www.varioptic.com).
14. B. Berge, "Liquid lens technology: principle of electrowetting based lenses and applications to imaging," Proc. of the MEMS 2005, pp. 227–230 (2005).
15. S. L. Cooper, S. A. Visser, R. W. Hergenrother, and N. M. K. Lamda, "Polymers," in *Biomaterial Science: an Introduction to Material in Medicine*, 2nd ed. (Elsevier Academic, 2004), Chap. 2, p. 78.
16. H. B. Lee, S. S. Kim, and G. Khang, "Polymeric biomaterial," in *The Biomedical Engineering Handbook* (CRC Press, in cooperation with the IEEE Press, 1995), Section IV, Chap. 42, p. 588.
17. J. D. Lytle, "Polymeric optics," in *Handbook of Optics* (McGraw-Hill, 1995), Vol. II, Chap. 34, p. 34.7.